The evolution of methane production rates from young to mature thermokarst lakes

Yarden Gerera[1], André Pellerin[2], Efrat Eliani Russak[1], Katey Walter Anthony[3], Nicholas Hasson[3], Yoav Oved Rosenberg[4], Orit Sivan[1*]

1 Department of Earth and Environmental Science, Ben-Gurion University of the Negev, Beer Sheva, Israel

2 Institut des sciences de la mer, Université du Québec à Rimouski, Rimouski, Québec, Canada

3 Water and Environmental Research Center, University of Alaska Fairbanks, Fairbanks, AK, USA

4 Geological Survey of Israel, Jerusalem 9692100, Israel

*Corresponding author

ABSTRACT

Thermokarst lakes, formed by permafrost thaw in the Arctic, are hotspots for methane (CH_4) and carbon dioxide (CO_2) emissions, and are expected to double permafrost carbon emissions by the end of the century. While the implications of ongoing permafrost thaw on methane dynamics within these lakes have been modeled, here we provide empirical data on methane production dynamics as lakes evolve from young recently formed lakes to older lakes that have been present for hundreds of years. Sediment cores (up to 4 m long) were collected from the centers and thermokarst margins of a new thermokarst lake [Big Trail Lake (BTL), <70 years] and from an older thermokarst lake [Goldstream Lake (GSL), ~900 years] from the same interior Alaskan watershed. Highest methane production rates were observed in the uppermost sediments near the sediment-water interface at the thermokarst margins of both lakes, with a steep decrease with sediment depth into the talik. BTL exhibited elevated methane production rates, correlated with higher carbon lability for thermal induced reactions measured by Rock Eval analyses, and suggesting its potential use as a proxy for organics susceptibility for methanogenesis. In contrast, GSL displayed lower methane production rates, likely due to a longer period of organic matter degradation and reduced carbon lability. The integrated sediment-column methane production rates were similar (around 7 to 10 mol m^{-2} $year^{-1}$), primarily due to the thinner talik at BTL. Our data support the predictions that formation and expansion of thermokarst lakes over the next centuries will increase methane production in newly thawed Yedoma permafrost sediments, while methane production will decrease as taliks mature and labile organic matter is used up.

1

1. Introduction

Permafrost covers one quarter of the northern hemisphere (Obu, 2021; Zhang *et al.*, 2008). Significant warming of the Arctic and subarctic regions, with temperature increase of 2 to 5°C relative to pre-industrial levels (Post *et al.*, 2019), exacerbates the thawing of this permafrost. In turn, these soils, which are currently still a store of carbon, becomes a source of carbon to the atmosphere by emitting greenhouse gases (Schuur *et al.*, 2015). It is estimated that until the end of this century thaw, rapidly thawed permafrost areas will become an important source of greenhouse gasses (Turetsky *et al.*, 2020). Among these gasses, methane is expected to be a dominant driver of the circumpolar permafrost-carbon radiative effect, responsible for up to 70% of this effect (Walter Anthony *et al.*, 2018).

Methane release is expected to be highly significant in rapidly thawing permafrost beneath thermokarst lakes, which are methane "hotspots" on the landscape, and expected to double permafrost carbon emissions and increase associated radiative forcing effects by 130% by the end of the century (Elder *et al.*, 2021; Hugelius *et al.*, 2014; Olefeldt *et al.*, 2016; Walter Anthony *et al.*, 2018). Thermokarst lakes initiate when ground ice melts and water accumulate in subsidence areas (Hopkins, 1949). As thaw continues beneath the lake, previously frozen organic carbon within the *in situ* thawed permafrost soils (called taberites (Farquharson *et al.*, 2016; Strauss *et al.*, 2013), becomes available for microbial degradation, which produces carbon dioxide and methane (Freitas *et al.*, 2025; Heslop *et al.*, 2015; Walter Anthony *et al.*, 2018). Particularly, organic-rich permafrost Yedoma soils of Alaska and Siberia are noteworthy reservoirs of old, ^{14}C-depleted, labile soil carbon that is quickly degraded into greenhouse gases upon thaw (Dutta *et al.*, 2006; Estop-Aragonés *et al.*, 2020; Knoblauch *et al.*, 2018; Zimov *et al.*, 1997).

Models have simulated the changes in methane production as thermokarst lakes evolve (Kessler *et al.*, 2012). These models show that while older lakes may have lower surface production rates, their taliks can still contribute significantly to total methane flux. Over centuries the talik deepens through the Yedoma and into the bedrock, while intra-talik organic carbon in the *in situ* thawed Yedoma sediments (taberites) gradually becomes refractory. At later stages, thawed permafrost organic matter is no longer available for methane production and the lake is no longer a strong source for permafrost-derived methane to the atmosphere, unless permafrost soil carbon

is retransported from lake margins or the watershed to surface lake sediments (Walter Anthony *et al.*, 2014).

However, while the implications of ongoing permafrost thaw on methane dynamics within these lakes have been modeled, few empirical data exist on changes in methane production in relation to stages of thermokarst-lake evolution. The limited studies on methane production rates in the talik of thermokarst lakes in the Arctic exhibit substantial variability, with fluctuations of 3 to 4 orders of magnitude observed across different environments and studies. For example, the top sediment layer of a non-Yedoma lake on the North Slope of Alaska shows methane production levels of 1000 nmol cm^{-3} d^{-1} (de Jong *et al.*, 2018). Methane production rates range from 2 to 35 nmol cm^{-3} d^{-1} in Doughnut and Vault Lakes in discontinuous Yedoma's permafrost in Alaska (Martinez-Cruz *et al.*, 2018), while values as high as 350 nmol cm^{-3} d^{-1} have been reported in Vault Lake (Heslop *et al.*, 2015), and lowest in Goldstream Lake (Sepulveda-Jauregui *et al.*, 2015). Our recent study in this region on short sediment cores (up to one meter depth) constrained methane production rates in the upper sediments similar to (Martinez-Cruz *et al.*, 2018), based on radiocarbon and methane accumulation incubations (Pellerin *et al.*, 2022). Freitas et al. (2025) showed, by using radiocarbon dating, sediment incubations, and sediment facies classifications, that methane production can also occur deep (~20 m) beneath yedoma thermokarst lakes in sand and gravel layers. All together, the data raised several questions regarding the evolution of methane production rates throughout the talik, the role of methane oxidation and the lability of organic matter in thermokarst lake systems that need further investigation.

Here, Yedoma's thermokarst lake sediment cores were retrieved up to four meters depth to measure, calculate and compare methane production rates along the talik ~~and its whole column accumulated rates (outward fluxes)~~ to compare between two distinct lake systems. Then the rates, indicating the susceptibility of the organics for microbial degradation by methanogenesis, were compared to the total organic carbon (TOC) and its lability for thermal induced reactions. The thermal lability was deduced from Rock-Eval analysis, which involves gradual heating under pyrolysis conditions, followed by combustion of the residual sample (Behar *et al.*, 2001). With the gradual heating, the generation of hydrocarbon, CO and CO$_2$ are monitored. Following pyrolysis, the residual organic matter is lean in hydrogen and structural changes making it more

3

aromatic and refractory. The long cores enabled a direct comparison of methane production rates, porewater geochemistry and organic matter lability along geographically proximate yet geomorphologically distinct lakes – a young lake (<70 years) and an old lake (~900 years) (Fig. 1). They also improved our understanding of how rates, carbon lability and methane ~~fluxes~~ production are expected to change over time, providing the first empirical data for comparison to model predictions.
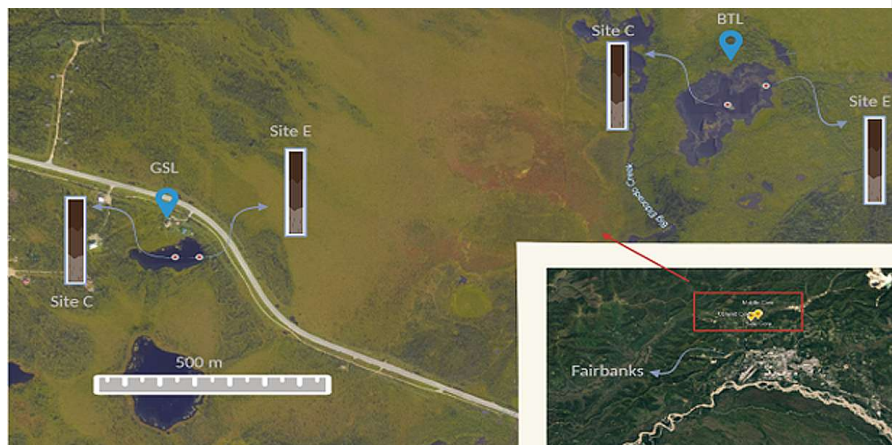

Figure 1: Study sites: The young (~70 years old) Big Trail Lake (BTL) and the old (850-900 years old in its center) Goldstream lake (GSL) in the Goldstream Valley (© Google Earth), including the locations of the collected cores in both lakes (Edge (E), Center (C)).

2. Methods

Region of study

The Goldstream Valley watershed is located about 10 km northeast of Fairbanks, Alaska (Fig. 1). This area has a subarctic, continental climate with an average annual temperature of -3.3°C and annual precipitation of 280 mm (Douglas *et al.*, 2020). The vegetation is primarily composed of boreal lowland species. The emergent lake and nearby thermokarst environments have been described by (Elder *et al.*, (2021). Recent studies (Hasson *et al.*, 2022) show that the mean annual ground temperature of permafrost is -0.26°C at a depth of 7.2 m. The Goldstream valley features discontinuous, ice-rich Yedoma type permafrost, originating from late-Pleistocene loess deposits that were remobilized during the Holocene. These deposits form thick layers over relic Goldstream formations, altering the soil chemistry and ice volume distribution (Péwé, 1975). ~~Since~~ Between 1949 and 2009, the number of thermokarst

4

lakes in the valley has doubled~~, and~~ their total area increased by about 40% ~~by 2009~~
(Walter Anthony *et al.*, 2020). These lakes are interconnected by a shifting watershed
that feeds into the Tanana River, which is part of the Yukon River Basin.

In this study, two markedly different thermokarst lakes were studied. Big Trail Lake
(BTL) (64.9189N, 147.8212W, 609 m^2 in 2009) is an actively expanding lake formed
from a wetland and possibly a migrating fluvial channel sometime between 1949 and
1967 (Walter Anthony *et al.*, 2020). Extensive geophysical surveys at BTL showed
massive ice (*e.g.* foliated ice wedges) starting roughly at 10-15 m below the irregular
talik shape (Walter Anthony *et al.*, 2020). Permafrost and valley hydrology were
investigated on the valley scale (Emond *et al.*, 2018). BTL is surrounded by valley-
bottom creeks and streams, some supply water to the lake by draining surrounding
upland fens and the historical channel; these tributaries sometimes run dry and isolate
the lake hydrologically at the surface. The outlet of the lake feeds into Eldorado Creek.

Goldstream lake (GSL) (64.9156N, 147.8495E, 1278m^2), located about 1.5 km from
BTL, is actively eroding into relic Yedoma permafrost with likely much less reworked
Yedoma, due to its location on the base toe slope of Goldstream valley and slightly
elevated above the Goldstream creek watershed at 196 m. Geophysical surveys
estimated talik thickness range of 30-40 m (Emond *et al.*, 2018; Péwé, 1975). A
previous study cored 20-m of Goldstream Lake sediments and found ice-free sand and
gravels beneath 16-m of thawed silt (Walter Anthony *et al.*, 2020). Radiocarbon dates
suggest the oldest part of the basin is around 850 to 900 years; however rapid expansion
of the eastern margin into ~~yedoma~~ Yedoma permafrost has occurred since 1949.

Sampling and profiles

We collected sediment cores using a vibro-corer deployed directly from the lake ice in
March 2022. In each lake one core was collected from the center of the lake and from
the edge within the water saturates zone ~~The core vibrated into the sediment over 1 to
2 minutes and the~~ with ~~-~~an aluminum liner. It was winched out of the sediment, tilted on
its side and cut into ~~1.5~~ ~1 m sections (marked in Table S1), which were quickly capped
and transported by ~~snow~~ a snow machine and ~~truck~~ vehicle to the University of Alaska
Fairbanks for further analysis. In the ~~lab~~ field, each ~~core~~ section was ~~opened~~ cut
lengthwise ~~sliced vertically~~ and one half was sampled horizontally at intervals of 15- to
25 cm ~~and sediment~~. First, a sub sample of sediment was taken immediately after slicing

5

the core liner for methane concentrations and ~~its~~ the stable carbon isotope composition ($\delta^{13}C_{CH4}$ and $\delta^{13}C_{CO2}$); about 1 mL of sediment was taken in a cut-off 1 mL syringe and inserted directly into a 20 mL fully saturated with an anoxic 5 M sodium chloride solution. Another cut-out 3 mL syringe was inserted as well into the sediment at each depth to extract sediment for incubations. For density measurements, samples were taken into 10 mL vials, weighed, and then re-weighed after drying an aliquot of sediment at 60°C for 4 days. For total organic carbon (TOC) concentration, its carbon stable isotope composition ($\delta^{13}C_{TOC}$) and Rock-Eval analyses a sediment subsample was freeze-dried. Porewater was extracted by Rhizons (Dickens *et al.*, 2007). The Rhizons were inserted into the sediment and vacuum was created with a 10 mL syringe which accumulated the extracted porewater after filtration in 0.22 μm. The filtrated porewater was then stored at 4°C in 2 -mL amber glass vials without headspace for measurement of dissolved inorganic carbon (DIC) concentrations and its stable carbon isotope composition ($\delta^{13}C_{DIC}$) within a week after the sampling.

Production rate experiments

A 3 mL cut-out syringe was inserted into the sediment in each core at 20 to 30 cm intervals to retrieve about 2 mL of sediment. The sediment was added to 20 mL serum bottle, which was sealed with butyl rubber stopper and crimped with aluminum cap. The bottles were vigorously shaken immediately and purged with 99.999% N_2 gas for 15 minutes to remove oxygen and other gasses. Three serum bottles were taken at each depth. After weighing, the samples were stored in the dark at 4°C. The increase in methane concentrations in the headspace was recorded after 80, 130 and 160 days by GC-FID (see below), allowing for the back-calculation of methane production rates.

Methane production rates were measured at each time point (80, 130, 160 days) using a small (100 μL aliquot) of gas from the headspace of the serum bottles. Headspace methane concentration was converted to total methane in the bottle based on the concentration, the volume of sediment and the volume of headspace in each serum bottle. Methane production rate was then taken as the increase in methane concentration over time. Since each depth had three serum bottles, the average methane production rate was reported for each depth and the uncertainty on methane production rate was reported as the standard deviation of the mean. After 160 days, $\delta^{13}C_{CH4}$ was also measured. Since any methane dissolved in the porewater at the time of sampling had

been removed during the N_2 purge, the $\delta^{13}C_{CH4}$ values represent the newly accumulated methane during the incubation.

Total profile methane production rates, ~~(fluxes,~~ reported in mol m^{-2} year^{-1}) were calculated using the methane production rates obtained from the incubation experiments and depth integration throughout the thawed talik. The inferred talik thickness was based on geophysical surveys and measurements of the taberite depth (Freitas *et al*., 2025; Walter Anthony *et al.*, 2020).

Analytical methods

The headspace of the serum bottles of the methane rate incubations was measured for methane concentrations at each time point using the procedure described by Pellerin et al. (2022). In general, ~~100~~ 250 µL aliquot of gas from the headspace and inserted into a Gas Chromatograph (~~Thermo~~ GC, Thermo) equipped with Flame Ionization Detector (FID) ~~(Thermo)~~ and a Packed ShinCarbon ST column (Restek) at ~~50~~120°C. The GC-FID was calibrated with a standard curve ~~of~~ prepared with methane concentrations ~~(of 1%)~~. Methane concentrations in the profiles were measured by injecting 3 mL of 99.999% N_2, while simultaneously removing 3 mL of the saturated 5 M sodium chloride solution. After equilibrating for two weeks upside down, bottles were vigorously shaken and analyzed for methane as descried above. This method had a precision of ±2 µM. The $\delta^{13}C_{CH4}$ and $\delta^{13}C_{CO2}$ values were measured together by PreCon and Gas Bench II interface ~~of~~ d with Delta V Gas Source Isotope Ratio Mass spectrometer (GS-IRMS, Thermo). I ~~with standards referred to the~~ of Vienna Pee Dee Belemnite (VPDB)nternal standard of Tiso-2 (Isometric Instruments, 2.5% CH_4) $\delta^{13}C$ -38.3 ‰, and inhouse (99.8 % CH_4) $\delta^{13}C$ -48.6 ‰ were used, with analytical error of 0.2 ‰. For $\delta^{13}C_{CO2}$ determination, 99.8 % CO_2 lecture bottle (Scott mini mix) with $\delta^{13}C$ of -25.5 ‰ was used and results are reported with analytical error of 0.3 ‰. ~~and an analytical error of ±0.2‰.~~All $\delta^{13}C$ results were reported compared to Vienna Pee Dee Belemnite (VPDB).

The TOC in the freeze-dried sediment was measured after the removal of carbonates by the addition of 1% H_3PO_4 and drying at 40°C in silver cups until the sample stopped reacting with the acid. Triplicate samples and internal standards were then packed in tin cups and measured on an elemental analyzer and HS2022 IRMS (Sercon). TOC concentrations were measured using concentration calibration and peak heights, and $\delta^{13}C_{TOC}$ were measured against VPDB with the reference materials IAEA-600 ($\delta^{13}C$ -

27.7 ‰ VPDB), USGS62 ($\delta^{13}C$ -14.8 ‰ VPDB) and USGS63 ($\delta^{13}C$ -1.2 ‰ VPDB). The precision was ±0.3‰.

Organic carbon lability for thermal induced chemical reactions was characterized by Rock-Eval analysis (Rock-Eval 6 Vinci Technologies). The technique determines the proportion of pyrolysable C (PC) and residual carbon (RC). PC is composed of the sum of three pyrolysates: S1, composed mostly of small volatile molecules, S2, larger hydrocarbon molecules thermally cracking like algal cell walls and S3, derived from oxygen-containing molecules. The residual carbon (RC) is released from the sample during the combustion cycle (Carrie *et al.*, 2012, Sanei *et al.*, 2005). The indices used as proxies to the organic lability are: 1) hydrogen index, which is calculated as HI = S2/TOC x 100 (Behar et al, 2001). Higher HI values indicate a greater hydrogen-rich organic compounds, implying lability. 2) The ratio between PC and RC. Higher ratio indicates that the OM is richer in hydrogen and is more aliphatic; hence, it might be more available to microbial respiration. About 20 mg of the prepared samples were placed in the RE6, which was then ramped at a predetermined rate (25 ˚C/min) from 200 ˚C to 650 ˚C in the pyrolysis oven. The oven was cooled down and the sample was transferred to the combustion oven, where it was ramped from 200 ˚C 0 ˚C up to 850 ˚C at a rate of 25 ˚C/min.

The DIC and $\delta^{13}C_{DIC}$ were analyzed after acidification of the porewater sample to convert DIC to CO_2. The $\delta^{13}C_{DIC}$ measurements used the GS-IRMS (Thermo) interfaced to Gas Bench II. Values are reported relative to VPDB with precision of ±0.1‰. DIC concentrations were measured by integrating the signal of the sample on the IRMS. The signal was calibrated using peak heights of a series of standards$NaHCO_3$ solutions prepared at concentrations of 3 to 10 mM. The precision was ±0.2 mM.

The comparison of $\delta^{13}C_{CH4}$ between the methane in the profiles and methane produced in the rate incubations was used to quantify the contributions of methane in the shallow sediments relative to the transport flux of methane migrating or diffusing from deeper in the talik. This is assuming that the methane measured in the profiles represents methane that is produced *in situ* plus methane that is produced in greater depths and migrates upward, while that in the incubations (after purging) represents only the *in situ* methane production. The bubbles composition was assumed to be the most negative

$\delta^{13}C_{CH4}$ value measured in the profiles because it migrates from deeper in the sediment, as was shown previously (Pellerin *et al.*, 2022).

Equation 1:

$$new\ CH4\ production\ fraction = \frac{\delta^{13}CH_4(PW) - \delta^{13}CH_4(bubble)}{\delta^{13}CH_4(incubation) - \delta^{13}CH_4(bubble)}$$

3. Results

Methane production characteristics from porewater profiles

Microbial respiration was intensive in general, as indicated by the high DIC concentrations in all sites. In the center of BTL DIC showed a linear increase from the surface towards 150 cm depth with a peak of 37 mM at 200 cm, followed by a subsequent decrease back to 25 mM (Fig. 1A2A). On the other hand, at the edge of BTL, the DIC ranged between 10 to 15 mM (Fig. 1B2B). Along the talik in the center of the lake the $\delta^{13}C_{DIC}$ values increased from 3 ‰ to 16 ‰ (Fig. 1A2A). On the edge of the lake the $\delta^{13}C_{DIC}$ values increased in the upper 50 cm from 5 to 17 ‰ and then remained relatively similar (Fig. 1B2B).

BTL center exhibited methane peaks at 70 and 300 cm (around 1 mM), while the remaining core sections showed methane concentrations ranging from 0.3 to 0.5 mM. The $\delta^{13}C_{CH4}$ values ranged from -55.6 permit to -69 ‰ in the deeper section (Fig. 2A). Methane concentrations at BTL edge (Fig. 2B) exhibited values of 0.2 to 0.5 mM at depths of 0 to 150 and 200 to 300 cm, with peak values of up to 1.4 mM observed at depths of 150 and 350 cm. The shallow part exhibited $\delta^{13}C_{CH4}$ values of -55 ‰, which became more negative, -71.5 ‰, in the deeper section.
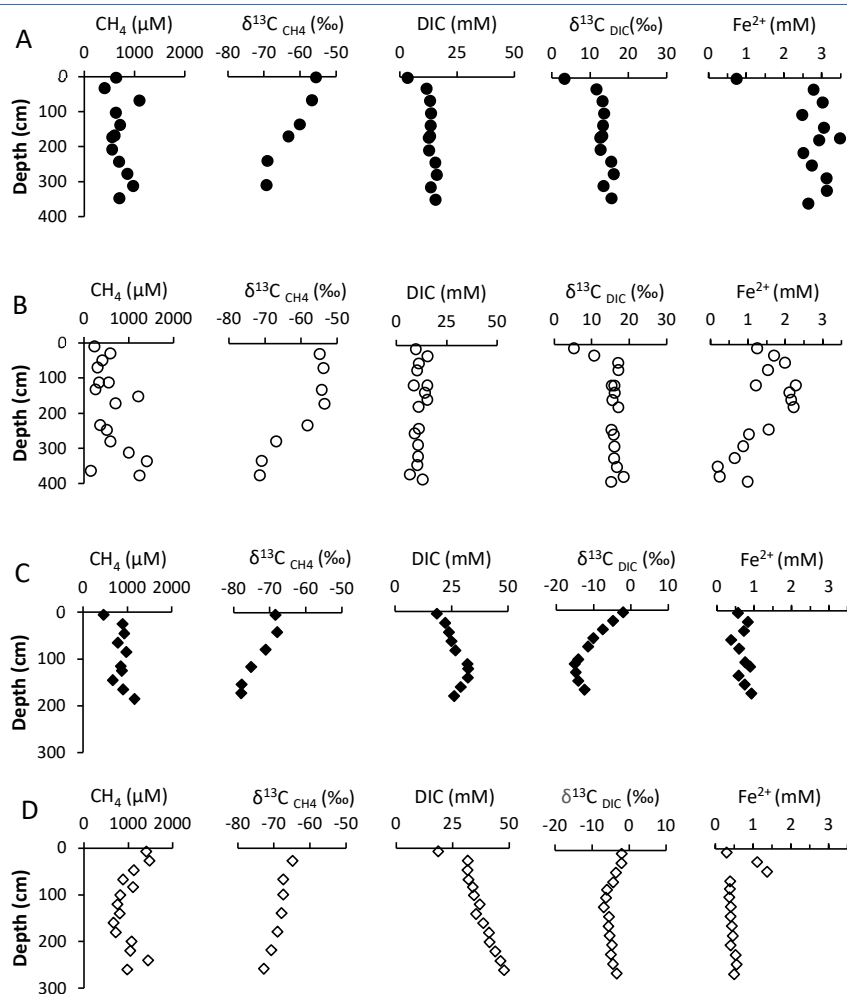
At GSL center, DIC concentrations remained around 20 mM, with a maximum of 32 mM observed at depth of 100 to 150 cm (Fig. 2C). The $\delta^{13}C_{DIC}$ values decreased in the upper 100 cm, ranging from -2 to -15 ‰, followed by a slight increase to approximately -12 ‰ (Fig. 2C). At the edge of GSL, DIC concentrations exhibited a linear increase with depth, ranging between 20- to 46 mM (Fig. 2D). The $\delta^{13}C_{DIC}$ values (Fig. 2D) showed different trends than BTL, with negative values, decreasing from approximately -2 to- -6 ‰ within the first 100 cm. Below this depth, there was a slight increase in $\delta^{13}C_{DIC}$ values, reaching -3 ‰.

249
250
251
252
253
254
255
256
257
258
259
260
261
262
263
264
265
266
267
268
269
270
271
272
273
274
275
276
277
278

Methane concentrations at GSL remained relatively steady at the center (1 mM), with a slight decrease at 150 cm to 0.7 mM (Fig. 2C). Methane concentrations edge exhibited varied range of 0.5 to 1.5 mM (Fig. 2D). The highest methane concentration was observed in the deepest and shallowest parts of the core (close to 1.5 mM). The lowest concentration was found at a depth of 150 cm. The $\delta^{13}C_{CH4}$ values at the center of GSL ranged from -68.4 ‰ in the shallow part to -78 ‰ in the deeper part (Fig. 2C). At the edge they ranged from -65 ‰ in the shallow part to -73 ‰ in the deepest section (Fig. S32D).

In conclusion, topSurficial sediments of lakes edges were organic rich (TOC~10 %) with relatively low $\delta^{13}C_{TOC}$ (table S1) and low methane and DIC concentrations. The TOC content decreased significantly with depth at the edges, while the center of the lakes had low organic content, as was measured all along the cores. In BTL in both edge and center, the $\delta^{13}C_{DIC}$ increased significantly with depth, with values typical of methanogenesis with concomitant increase of methane and DIC. In GSL, on the other hand, there was a significant decrease in $\delta^{13}C_{DIC}$ with relatively constant DIC values and methane concentrations and isotopes in the rate incubations, which suggest small role of methane related processes with some signature of methane oxidation in the upper sediments.

Need to remove the labels BTL and GSL and EDge and Center from the frigure axis labels :Commented [AP1]

279
280
281
282
283
284
285
286
287
288
289
290
291
292
293
294
295
296

A

CH$_4$ (μM)   δ^{13}C $_{CH4}$ (‰)   DIC (mM)   δ^{13}C $_{DIC}$(‰)   Fe^{2+} (mM)

Depth (cm)

B

CH$_4$ (μM)   δ^{13}C $_{CH4}$ (‰)   DIC (mM)   δ^{13}C $_{DIC}$ (‰)   Fe^{2+} (mM)

Depth (cm)

C

CH$_4$ (μM)   δ^{13}C $_{CH4}$ (‰)   DIC (mM)   δ^{13}C $_{DIC}$ (‰)   Fe^{2+} (mM)

Depth (cm)

D

CH$_4$ (μM)   δ^{13}C $_{CH4}$ (‰)   DIC (mM)   δ^{13}C $_{DIC}$ (‰)   Fe^{2+} (mM)

Depth (cm)

299

299

300

301

302

303

304

305

306

307

308

309
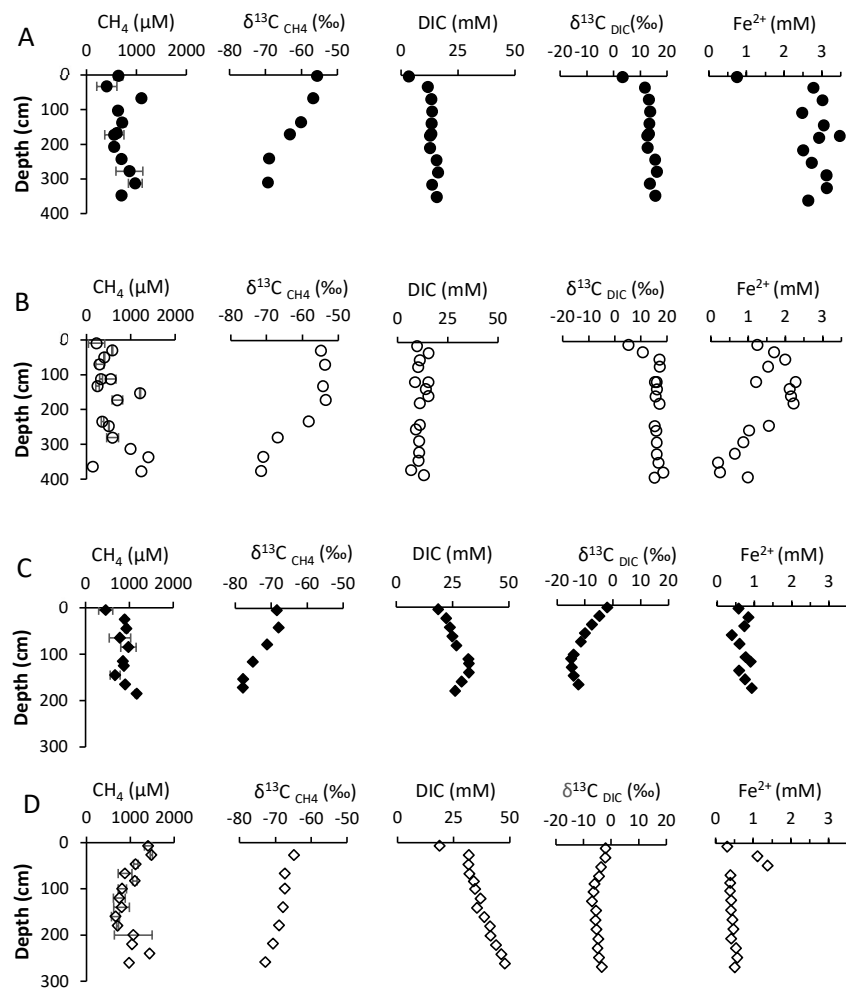
Figure 2: Pore water profiles of GSL (circles) and BTL (diamonds) cores. Panels A and B correspond to ~~BTL Center (full) and Edge (empty) respectively,~~ while panels C and D correspond to GSL Center and Edge respectively. ~~For dissolved inorganic carbon stable isotopes of carbon, note the different scales between the lakes.~~ Error bars within markers limit unless depicted otherwise.

310
311
312
313
314
315
316

Methane production rates in sediment incubations

Methane production rates were measured by sediment incubation batch experiments. The sediment from BTL and GSL had the highest methane production rates near the sediment-water interface. In BTL the rates within the upper meter ranged between 2 and 20 nmol cm^{-3} day^{-1} in the core taken from the center of the lake (Fig. 3A) and 7 to 35 nmol cm^{-3} day^{-1} in the core taken from the edge of the lake (Fig. 3B). In the deeper sediments, the rates decreased to about 1 nmol cm^{-3} day^{-1} in both sites.

At the center of GSL (Fig. 3C), methane production rates were of 4 to 6 nmol cm^{-3} d~~ay~~ay^{-1} in the upper one meter of sediment. Deeper, the rates decreased, ranging from 2 to 4 nmol cm^{-3} day^{-1}. At the edge higher rates were measured in the upper 50 cm (but lower than in BTL) following by a sharp decrease below 50 cm depth (Fig. ~~4~~3D).

Methane production rate (nmol cm^{-3} d^{-1})
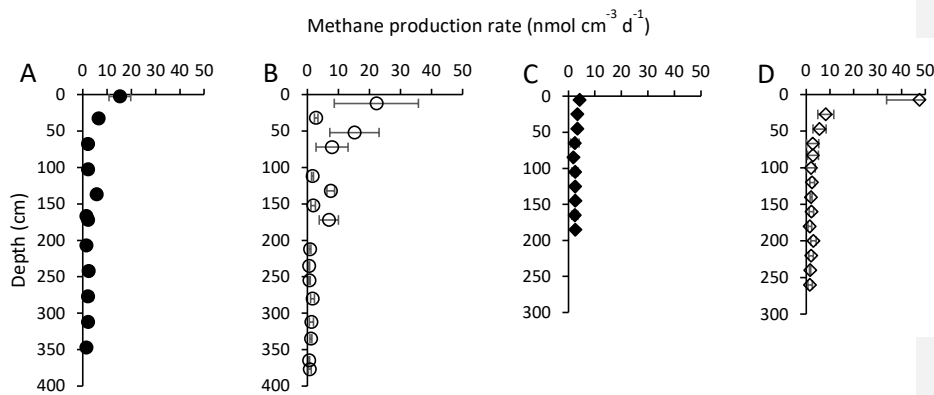
Figure 3: Methane production rates (nmol CH_4 cm^{-3} day^{-1}) from incubation experiments of BTL sediments: Center (A) and Edge (B) cores. A steep decrease in rates with depth is observed in both the edge and center sites. Depth to permafrost beneath Big Trail Lake is thought to be 10 to 15 meters (Walter Anthony et al., 2020). Methane production rates (nmol CH_4 cm^{-3} day^{-1}) in GSL from incubation experiments of Center (C) and Edge (D) cores. A noticeable decrease in rates with depth is observed at both center and edge of the lake. The talik depth in GSL is estimated in the center to be between 15 to 40 m (see below).

Total thawed talik methane production

The total profile-integrated methane production rate throughout the thawed talik ~~may be similar to can be used as a proxy for~~ indicates the potential flux~~es~~ of methane out of the sediment into the lake water column. This accumulated rate depends on methane production rates at individual depths, facies thicknesses (surface sediments, taberites,

13

etc.) and talik thickness. ~~S~~Since we did not have samples below 4 m depth, we extrapolated our data to the depth range of the known taberite thickness which was ~~in the talik (~~10 to 15 m at BTL and ~16 at GSL~~;~~ (Walter Anthony *et al.*, 2020). Different fits were tested for calculating the total methane production (Table S3-S5), and a power law regression was chosen as the best fit for extrapolating the total methane production rate ~~fluxes~~ (Table S4, Fig. ~~5)~~4).
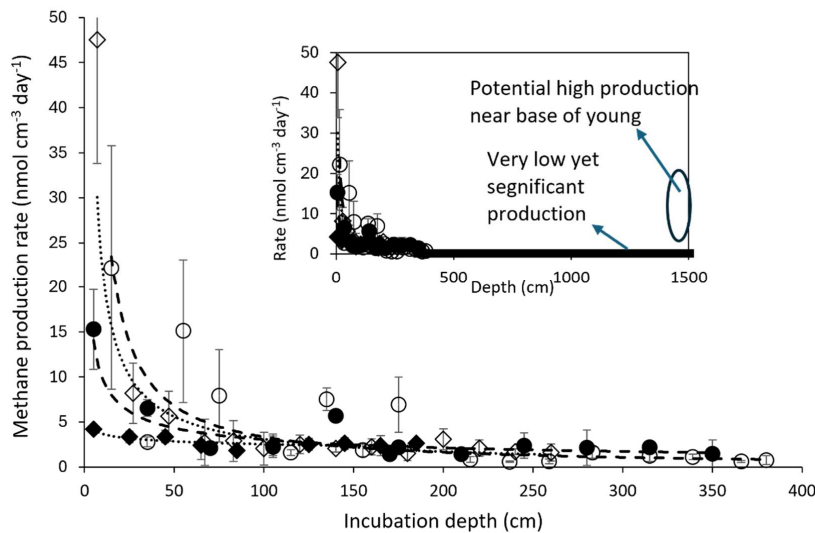
Figure ~~5~~4: Methane production rates as measured in the different cores (symbols) and power law extrapolation (curves, equations in Table S5) down to 4 meters and 15 meters (upper right side). A constant low rates of less than 1 nmol cm^{-3} day^{-1} below 3 meters down to 15 meters is also marked in the upper right side, as well as the potential role of high production of methane near of the base of the young talik.

The total 12 m column methane production calculated for the BTL edge and center cores were about 8.5 (±12%) and 7.4 (±37%) mol m^{-2} year^{-1}, respectively. In GSL, talik thickness is greater (<40 m); however, the volumes of thawed silt are potentially comparable at both lakes, and the main difference is in time since thaw. Because BTL is a younger lake, we assume the talik sediments have thawed within the last 70 years; whereas talik sediments beneath the center of GSL are thought to have been thawed for eight to nine centuries (Walter Anthony *et al.*, 2020). At GSL lake our 15 m profile-integrated methane production rates from the center and the edge were 7-11 mol m^{-2} ~~y~~year^{-1} (Table S4). Large uncertainties stem from the extrapolation (Table S5), the very

long tail followed by the real measurements (Fig. 54), potential variability in the composition and thickness of the surface organic-rich sediments and the actual talik depth across both lakes. We also assume that the rates are very low down to the base of the talik, whereas there is a potential for high production rates near the base of the young taliks. These high rates together with the high surface rates in the edges of the lakes and the center of BTL can explain the ebullition there and the lack of ebullition at the center of GSL (Walter Anthony *et al.*, 2020).

The source of methane

The source of methane in the sediment was ~~calculated roughly~~estimated by comparing the $\delta^{13}C_{CH4}$ values in the profiles to those measured in the rate incubations (after purging and waiting several months for *in situ* production) (Fig. S2S1). The $\delta^{13}C_{CH4}$ values in the profiles from BTL were around -55 to -75 ‰ (Edge) and -60 to -70 ‰ (Center), whereas the values from the incubations of sediment from BTL were about 10 to 20 ‰~~permilles~~ higher (~~heavier~~ enriched in ^{13}C) all along the profiles. The same observation is made in GSL, where $\delta^{13}C_{CH4}$ values of the dissolved methane in the profiles were around -60 to -70 ‰ (Edge) and -70 to -80 ‰ (Center), with more positive values for incubations. The significant difference between the incubations and *in situ* profiles points towards an additional deep source of light methane in the natural environment, consistent with talik-sourced ebullition observations (Walter Anthony *et al.*, 2020).

Organic carbon characteristics in the sediments

The TOC profiles in the center of BTL sediments showed a gradual decline from 2% to less than 1% and in GSL from around 1% (Fig. S3S2). At the edge of the lakes higher TOC was observed near the top of the cores, reaching levels of up to 13% (BTL) and 9% (GSL) and gradually decreasing with depth. The $\delta^{13}C_{TOC}$ in the center was constant near -27 ‰ in the upper 150 cm (Table S1). An increase was observed around 200 and 350 cm, reaching -25 ‰. At the edge, $\delta^{13}C_{TOC}$ values were around -28 ‰ at the upper part with an increase observed below 200 cm to -25 ‰.

Rock-Eval data obtained at both center and edge sites of both lakes showed a correlation between organic index values and sediment depth. The HI of the BTL was mostly much higher from that of the GSL and is indicative for a mix of Type I-III kerogen for the young lake (BTL), and a Type III kerogen for the mature lake (GSL). The OI on the

15

other hand was very high for both lakes, exceeding 150 mgCO$_2$ g^{-1}TOC. In both the edge and center cores of the BTL there was an inverse dependency between the HI and OI, suggesting that with the lose of H the OM became more oxidized. This relation is missing from the mature lake, in which the OM lost most of its H, presumably due to microbial degradation (Fig. ~~S4~~S3). PC/RC ratio in both sites of BTL decreased with depth and stabilized at 250 cm, with the center core generally exhibiting lower ratios compared to the edge. The PC/RC ratio in the edge of GSL slightly decreased with depth. When comparing the two cores the lower values were observed at GSL center core, meaning it is more refractory than the edge (Fig. ~~6~~5).
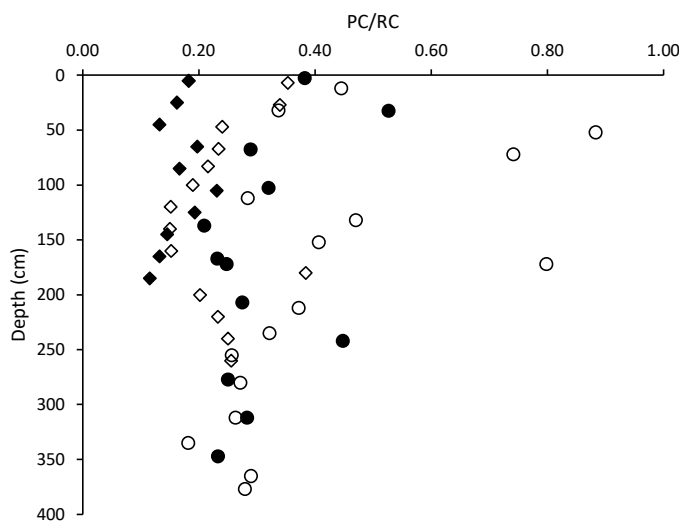
Figure ~~6~~5: Sediment profiles of the ratio of pyrolysable carbon to refractory carbon (PC/RC). The ratio decreases not only with depth but also with the evolution of the lakes, as organic matter becomes more refractory. The uncertainty of the data is smaller than the symbol (~~Circles~~ circles – BTL, ~~Diamonds~~ diamonds – GSL, full symbols – Center, Empty symbols – Edge of lakes).

4. Discussion

Total methane production in the talik

The methane production rates observed in the upper sediments of this study are similar in magnitude to the ones observed in our previous studies (Lotem *et al.*, 2023; Pellerin *et al.*, 2022). Previous studies in which cores depth was limited to about one-meter

depth were unable to provide a full understanding of the characteristics of methane dynamics within thermokarst lake taliks. In Vault Lake, another thermokarst lake in central Alaska, a decrease in methane production was observed with depth down to 6 m but methane production rates were significantly higher than most reports (Heslop *et al.*, 2015). (Freitas *et al.*, (2025) also showed low, but significant cumulative anaerobic respiration throughout the taberal sediments down to the gravel zone at around 16 m in GSL, with scattered values below.

Since we were able to sample up to 4 m in the talik of both BTL and GSL and both in the center and the edge (near the lakeshore) locations, our rates measurements provide important confirmation of conceptual and numerical model predictions. They show high methane production rates in the surface with steep decrease with depth in the talik as the taberite organic matter becomes more refractory over time. Our findings are also consistent with the findings from 8 m permafrost sediment core from the Lena Delta where highest methane production rates were observed in the first 125 cm (Wagner *et al.*, 2007).

The study also serves as the first empirical test of models predicting changes in methane production rates and fluxes with the evolution of lakes. It shows that methane production rates are highest in the top sediments and are low, but still significant in the deep talik. Indeed, tWe did not measure here is no significant difference between methane production rates at depths deeper than 100 cm at BTL and GSL (Fig. 54). However, other lines of evidence such as the different isotopic enrichments of the DIC pools strongly suggest that While there are should be significant differences in methane production rates between BTL and GSL. It may be that, the low rates and higher uncertainty on the measurements in the deep talik made it impossible to differentiate between themthe rates in the two lakes.

The long cores and the steep methane production decrease with depth enable estimating the total production rates with higher certainty than the accumulated rates calculated in the 1 m cores and estimated constant rates along the talik (Pellerin *et al.*, 2022). It should be noted that despite reaching down to 4 m in the talik, we still needed to extrapolate the rates to the entire thickness of thawed taberal sediments which is (10 to 16 m depths, (Walter Anthony *et al.*, 2020). It has been suggested previously that methane production rates may increase with depth of the talik because more recently

17

thawed permafrost might release more labile organic matter available for degradation (Walter Anthony et al., 2014) due to a rapid turnover time upon thaw (Schadel *et al.*, 2014; Shaver *et al.*, 2006). However, previous studies have not found a significant rise in methane production rates with depth, except near the thaw front at the base of the young talik (Heslop *et al.*, 2015). This potential rise in young talik is marked in fFigure 6, and may explain the lowest accumulated production rate fluxes at in the center of GSL. The recent study of (Freitas *et al.*, 2025) showed similar low values in the taberites overlying the sand/gravel zone in GSL at about 16 m and then scattered high values (in part because they were normalized to the total organics that was very low). In order to extrapolate our rates deeper into the talik, we experimented with several approaches such as using power law decay or constant rate that reflects the lowest lower rates obtained in the incubations. Using the integrated rates with a power law equation, we calculated total talik methane production (Table S4). We decided to present a power law fit since it indicates a declining rate in the deeper talik which we believe to be most realistic and reflects the overall trend observed in our incubations (Table S5). However, it is important to highlight that all models that we experimented with yield very similar conclusions as to the total talik methane production and the model used to extrapolate methane production rates deep in the talik does not affect our conclusions.

An important finding is that facies thickness and talik depth play a significant role in determining total talik methane production, and not just lake age and location within a lake. This is because despite measurably higher methane production rates in the first upper meter of sediment cores, as well as near the edges of the lakes, the low but relatively constant methane production rates observed at depths in all the sites (5- to 10%), impact the integrated total talik methane production rates (Fig. 74).

The new total thawed talik methane production rates are of the same magnitude as methane emissions measured by previous studies in BTL (Elder *et al.*, 2021) and other discontinuous permafrost thermokarst lakes (Fig. 76). This similarity supports only a minor role for methane oxidation (aerobically and anaerobically) in the lakes. It also fits the finding in the upper one meter of several thermokarst lakes, which shows that anaerobic oxidation of methane (AOM) rates, as deduced from batch experiments, are two orders of magnitude lower than methane production and not a significant sink of methane (Lotem *et al.*, 2023).

The implication of this observation is that as ~~the~~ lakes mature total thawed talik methane production rates can remain similar or even increase, although the carbon becomes less available for microbial degradation. This is ~~, if~~when the talik deepens fast enough~~, it~~ and ~~can~~ offsets the overall drop in carbon lability ~~and the total thawed talik methane production rates will remain similar or even increase~~. This is the case observed for both BTL and the eastern thermokarst margin of GSL. The question is whether there is control and a link between the organic carbon, its nature and methane production rates in BTL and GSL, as discussed below.

CH4 Flux (mol m-2 yr-1)
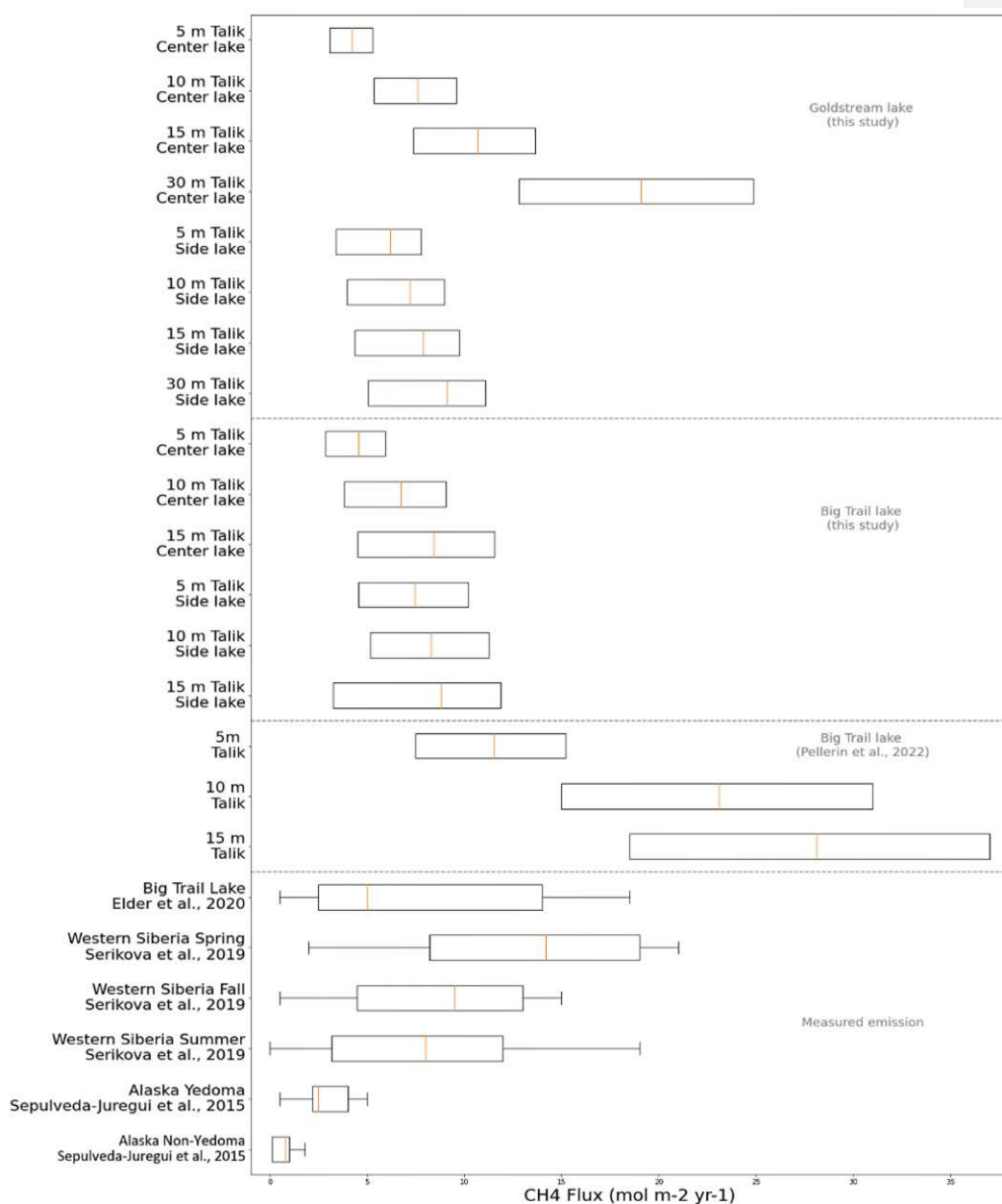
Figure 76: Total talik mMethane production fluxes from sediments to water column in BTL and GSL (mol m⁻² year⁻¹), obtained by integrating the methane production rates over the potential range of thawed talik depths in the sediments (from surface to the marked depth) using a power law extrapolation. The middle of the box corresponds to the mean estimate and the uncertainty is the length of the boxes.

Factors influencing methane production rates and potential net emissions

We investigated further the controls of methane production in BTL and GSL taliks. These lakes are in the same valley system, it seems very likely that they have the same sources, and that methane production will be influenced from *in situ* difference. As the isotopic composition is much more sensitive for quantifying sedimentary processes rather than the concentration changes (*e.g.* Sivan *et al.*, 2011), $\delta^{13}C_{DIC}$ and $\delta^{13}C_{CH4}$ can be used to determine the controls on methane production in the lakes. The first clear observation is that methanogenesis is strongly imprinted in the $\delta^{13}C_{DIC}$stable carbon isotope mass balance of the young, recently thawed talik of BTL, and much less sonot in older, GSL talik, which has been thawed longer (Fig. 2). This is indicated in Tthe $\delta^{13}C_{DIC}$ values of BTL, which are more positive (around +10 to 20‰) and reflect a stronger imprint ofas methanogenesis, which produces methane isotopically depleted in ^{13}C and, by mass balance, ^{13}C enriched DIC. than at The GSLt, where $\delta^{13}C_{DIC}$ values in the sediments of GSL are around -5 to -10‰ at depth (Fig. 2), as they are probably affected only by slight anaerobic oxidation of methane and other organics with mechanism discussed by Lotem *et al.* (2023).

The $\delta^{13}C_{CH4}$ values of both lakes of -78 to -53‰ (Fig. 2) support this picture. They are typical to freshwater sediments, which are usually dominated by microbial acetoclastic methanogenesis (*e.g.* Whiticar, 1986). Methanogenesis pathways and their importance in this system were quantified by radiocarbon probing (Pellerin *et al.*, 2022) and by the $\delta^{13}C_{CH4}$ vs δD_{CH4} (Liu *et al.*, 2025). The relatively heavy $\delta^{13}C_{CH4}$ values fit also to slight methane oxidation (*e.g.* Whiticar 1999; Sivan *et al.*, 2011), which results in enrichment in ^{13}C-CH$_4$. The control of methanogenesis on BTL profiles can be seen also by looking at the $\delta^{13}C_{CO2}$ values and plotting them against $\delta^{13}C_{CH4}$, similarly to Krause and Treude (2021) (Fig. Sxx7). The data support acetoclastic methanogenesis and methane oxidation in all sites.

This could stem from higher methane oxidation at GSL which would enrich in ^{13}C the DIC pool. It could also stem from DIC production by more energetically favorable electron acceptors such as iron oxides which are abundant in these sediments of both GSL and BTL. However, the higher rates of methane production are needed at BTL to produce the marked positive isotopic signature observed. This The main difference between the lakes is likely related to the fundamental difference in age of the two taliks,

which influences the lability of organic matter and the resulting biogeochemical cycles. ~~This~~The lability difference of the organics was further investigated by assessing the properties of the organic matter in the talik of BTL and GSL.
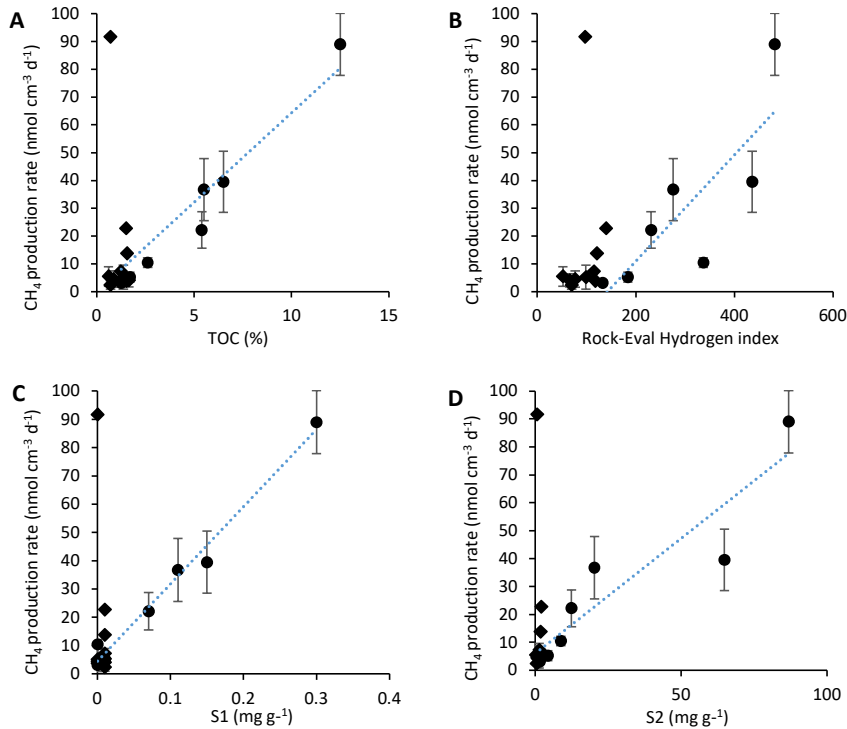
Figure ~~8~~7: Methane production rates (including its uncertainty) as measured in ~~the~~ ~~top~~ upper 100 cm from both center and edge cores ~~, and their correlation~~ compared with ~~to~~ TOC content (~~a~~A) , hydrogen index (~~b~~B, R2=0.67) and the most labile organic matter compounds: S1, S2 (~~c~~C, ~~d~~D), as measured on Rock-Eval. A positive relationship (R^2 0.67- to 0.98) is evident in the upper 100 cm for BTL (circles) but not for GSL (diamonds).

~~Methane~~ It can be seen that methane production rates are highly correlated to TOC and indices of thermal induced lability in the upper sediments (Fig. ~~8A~~7A), but not correlated with them ~~TOC and indices of thermal induced lability~~ in the deep talik of BTL (Fig. ~~S5~~S4-~~S6~~S5)~~, but they are highly correlated to these parameters in the upper sediments (Fig. 8A). In the upper 100 cm of BTL, the center and edge cores both show a~~The correlation ~~is evident~~ is between ~~the~~ two independent methods ~~to~~ that estimate ~~the~~ lability of ~~the~~ organic matter ~~organics~~ to microbial degradation - the lability based on

527
528
529
530
531

532
533
534
535
536
537
538

to thermal degradation induced reactions and the methane production rate. It can be seen that theThe highest hydrogen index and the most labile fraction of pyrolyzed carbon (S1, S2), are correlated with methane production rate in both center and edge sites (Fig. 8B-D7B-D). The results demonstrate that the highest methane production rates observed in our study, in the top meter of BTL are likely driven bydue to both the lability and quantity of organic carbon.

The pyrolyzed carbon to residual carbon ratio (PC/RC) is a simple measure of how labile the organic matter is. As the PC/RC ratio higher, the sample has more hydrogen, and has more pyrolysable fraction (Carrie *et al.*, 2012). Throughout the four cores taken for this study, the RC/PC ratio was highly dependent on depth in the talik (Fig. 65), which is consistent with older, less labile organic carbon deeper in the sediment as a result of depositional history. However, the most interesting observation was the decreasing trend of lability to thermal induced reactions between sites. BTL edge had the highest PC/RC values which correspond to organic matter with the highest lability, followed by BTL center, GSL edge, with the lowest value observed at the GSL center (Fig. 65). The lake edges exhibit highest PC/RC ratios compared to the centers of the lakes, suggesting that the centers of the lakes contain more refractory organic matter, which may be a result of the edges of the lakes being "younger" (meaning they the age since thaw)have been thawed for less time. Alternatively, it could be that the edges have additional input of organic matter from vegetation or runoff from land, as supported by the labile fractions found in the edges (Fig. 8C7C). Both edge and center of GSL, on average, had lower PC/RC ratios than both the center and edge of BTL. This is interpreted as GSL containing a greater fraction of less labile organic matter, consistent with the longer time since the permafrost thawed and formed the talik and lake at this site. Carbon thus becomes less labile for microbial degradation as the lake evolves. In permafrost environments, organic matter lability is not always correlated directly with what is termed the "age" of the organic matter such as in most marine sediments where lability, depth and age are often directly correlated. In the talik of thermokarst lakes, time since thaw seems to have some control on the lability of the organic matter and exerts control on methane production rate.— All together, our study emphasizes the potential use of the lability of thermal induced reactions as a proxy for organics lability for methanogenesis.

539
540
541
542
543
544
545
546
547
548
549
550
551
552
553
554
555
556
557
558
559
560
561
562
563
564
565
566
567
568
569
570

Formatted: Font: Italic, Complex Script Font: Italic

23

It seems thus that at the onset of thawing, during the formation of a young thermokarst lake a high amount of highly labile organic matter accumulates and begins to degrade. As thawing progresses, the lakes margins expand and deepen and the refractory organics remain, leading to lower methane production rates. A proposed conceptual mechanism is presented in figure 98. This mechanism can be tested in future studies, which include expanding the study to additional lakes, incorporating seasonal sampling, and integrating microbial community analyses to better understand methane cycling processes.

Figure 98: Laboratory incubations support the conceptual and numerical models of decreasing carbon lability leading to lower methane production as yYedoma thermokarst lakes mature. The gray sediment denotes yYedoma permafrost soil. Red scale color denotes organic matter lability with talik expansion into in-situ thawed yYedoma (taberites). (A) Young active lake: Labile carbon results in high methane production rates with methane production in taberites proportional to the talik thickness. (B) Expanding lake: Over decades new organic matter from surrounding soils and plants is added to surface lake sediments and to freshly thawed taberites at the base of the talik, while the availability of labile organic matter attenuates in formerly thawed taberites. (C) Mature lake: Over centuries the talik deepens (into bedrock) beyond the depth of taberites, while taberite organic carbon becomes refractory. Methane emissions may still be significant, depending on exogenous (non-taberite) inputs of organic matter. At later stages (as suggested by Walter Anthony *et al.*, 2014), the organic matter becomes no longer

24

available for methanogenesis and the lake thus is no longer a significant source for permafrost-derived methane to the atmosphere.

Methane origin in the talik

The comparison of $\delta^{13}C_{CH4}$ values between the profile measurements and those obtained from the incubation experiment shows less enriched $\delta^{13}C_{CH4}$ values in the sediment cores across all samples (Fig. S7S6). These values in the sediment profiles show that the pore water methane is not entirely produced *in situ*, suggesting that the new methane produced in the lake sediments contains a more isotopically enriched $\delta^{13}C_{CH4}$ values compared to the methane diffused from deeper layers, which could be produced by a different methane production pathway (Pellerin *et al.*, 2022; Liu *et al.*, 2025). Methane generated at greater depths within the talik, which subsequently ascends through diffusion or bubble transport, exhibits a more negative $\delta^{13}C_{CH4}$ probably due to different conditions from those prevailing in the top meter of the talik, possibly under lower metabolic rates and using different metabolic pathways (Maltby *et al.*, 2016; Berberish *et al.*, 2020; (Pellerin *et al.,* 2022).

By considering the less enricheddepleted $\delta^{13}C_{CH4}$ values in the sediment cores and the corresponding incubation values at each depth, we can quantitatively assess the fraction of modern methane present in the sediment profile. A comprehensive analysis of the young production fraction in all four cores showsing that as depth increases, the contribution of newly produced methane decreases and tends to approach zero across all cores (Fig. S7S6). Additionally, the new methane fraction observed in Goldstream Lake (both edge and center) is smaller compared to that of BTL. This finding suggests a shift towards a greater influence of newly produced methane in younger lakes compared to those that have formed and thawed longer. A shift in methanogenesis pathway in the sediments vs the incubations can be an alternative explanation, however less likely, given the observations here and in the previous studies (Pellerin *et al.*, 2022).

5. Conclusions

This study presents the first empirical data quantifying methane production and organic matter degradation of thermokarst lakes from young to mature. This study aimed to supply empirical data that test modeled evolution of methane cycling in thermokarst lakes. This was achieved by quantifying the evolution of organic matter degradation

25

and methane production rates throughout the evolution of lakes from a young dynamic lake to a mature one. The findings underscore the vertical variations in methane production rates, the influence of permafrost thawing on microbial activity, and the divergent patterns observed among lakes of different development stages.

Our high-resolution profiles and long-term incubations show highest methane production rates on the edges of the young lake BTL, then the center of BTL, then the edge of mature GSL and the lowest at the center of GSL. The higher rates coincided with higher TOC levels, more labile carbon content for thermal induced chemical reactions, simpler carbon compounds, and a more contribution of young methane source. These factors provided probably favorable conditions for microbial populations to decompose carbon, resulting in elevated methane production. The high correlation between the two different methods to estimate organic carbon lability for microbial degradation methane production rates and the lability to thermal induced chemical reactions, emphasizes the potential use of the Rock-eval analyses to estimate the susceptibility of organic matter for microbial degradation.
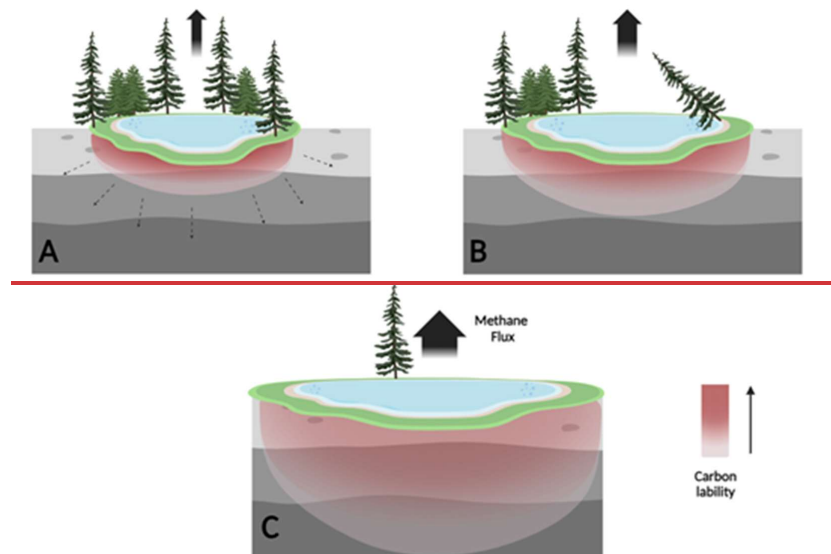
Figure 9: Laboratory incubations support the conceptual and numerical models of decreasing carbon lability leading to lower methane production as yedoma thermokarst lakes mature. The gray sediment denotes yedoma permafrost soil. Red scale color denotes organic matter lability with talik expansion into in-situ thawed yedoma (taberites). (A) Young active lake: Labile carbon results in high methane production rates with methane production in taberites proportional to the talik thickness. (B) Expanding

26

~~lake: Over decades new organic matter from surrounding soils and plants is added to surface lake sediments and to freshly thawed taberites at the base of the talik, while the availability of labile organic matter attenuates in formerly thawed taberites. (C) Mature lake: Over centuries the talik deepens (into bedrock) beyond the depth of taberites, while taberite organic carbon becomes refractory. Methane emissions may still be significant, depending on exogenous (non-taberite) inputs of organic matter. At later stages (not shown), the organic matter is no longer available for methanogenesis and the lake thus is no longer a significant source for permafrost-derived methane to the atmosphere.~~

~~Despite~~ While the higher rates in the upper part of the young lake, the increase in t~~facies thickness and t~~alik depth also play a significant role in determining the total methane production rate ~~fluxes~~. Our proposed conceptual mechanism, as depicted in figure 9~~8~~, considers these two parameters (lake age and thawed talik thickness) when discussing accumulated methane production rates. ~~At the onset of thawing, during the formation of a young thermokarst lake (A), a high amount of highly labile organic matter accumulates and begins to degrade. Methane production is particularly pronounced in the upper shallow part of the sediment. As thawing progresses, the lakes margins expand and deepen. Organic matter continues to accumulate at the top while its older fraction undergoes degradation in deeper parts, resulting in decreased lability (B). When the lake matures, the refractory organics remain, leading to lower methane production rates. Conversely, the talik deepens, ~~enhancing ~~resulting in production larger fluxes from older lakes (C).~~ It can be ~~predicted~~ expected thus that the exp~~ansion ending~~ of thermokarst lakes in the Arctic will continue to ~~have similar role in methane fluxes~~ influence methane production as the young~~er~~ lakes expand into deeper ~~and that the control on methane emission will be just the thickness of the~~ permafrost layer~~s~~.

Acknowledgments

Authors contribution

YG, AP, EER and OS participated in sampling campaigns led by KWA and NH. YG conducted incubation experiments. ~~YG and~~ EER and YG measured geochemical

27

samples and processed the data. NH conducted geophysical measurements. OS led manuscript writing with AP and KWA. YOR was responsible for Rock Eval6 method development and with AP and OS interpreted the data.

Conflict of interest

The authors declare that they have no conflict of interest.

SUPPORTING INFORMATION

Additional supporting information may be found in the online version of the article at the publisher's website.

References

Behar, F., Beaumont, V., and De B. Penteado, H. L.: Rock-Eval 6 Technology: Performances and Developments, Oil & Gas Science and Technology - Rev. IFP, 56, 111–134, https://doi.org/10.2516/ogst:2001013, 2001.

Berberish, M.E., Beaulieu, J/J/, Hamilton, T.L., Waldo, S., and Buffam, I.: the spatial of sediment methane production communities within ta eutrophic reservoir: Imoportance of organic matter source and quantity, Limnology and Oceanography, 65 (6), 1336-1358, https://doi.org/10.1002/lno.11392, 2020.

Carrie, J., Sanei, H., and Stern, G.: Standardisation of Rock–Eval pyrolysis for the analysis of recent sediments and soils, Organic Geochemistry, 46, 38–53, https://doi.org/10.1016/j.orggeochem.2012.01.011, 2012.

De Jong, A. E. E., In 'T Zandt, M. H., Meisel, O. H., Jetten, M. S. M., Dean, J. F., Rasigraf, O., and Welte, C. U.: Increases in temperature and nutrient availability positively affect methane-cycling microorganisms in Arctic thermokarst lake sediments, Environmental Microbiology, 20, 4314–4327, https://doi.org/10.1111/1462-2920.14345, 2018.

Dickens, G. R., Koelling, M., Smith, D. C., Schnieders, L., and the IODP Expedition 302 Scientists: Rhizon Sampling of Pore Waters on Scientific Drilling Expeditions: An Example from the IODP Expedition 302, Arctic Coring Expedition (ACEX), Sci. Dril., 4, 22–25, https://doi.org/10.5194/sd-4-22-2007, 2007.

Douglas, T. A., Turetsky, R. T., and Koven, C. D.: Increased rainfall stimulates permafrost thaw across a variety of Interior Alaskan Boreal ecosystems, Climate and Atmospheric Science, 3, https://doi.org/10.1038/s41612-020-0130-4, n.d.

Dutta, K., Schuur, E. A. G., Neff, J. C., and Zimov, S. A.: Potential carbon release from permafrost soils of Northeastern Siberia, Global Change Biology, 12, 2336–2351, https://doi.org/10.1111/j.1365-2486.2006.01259.x, 2006.

Elder, C. D., Thompson, D. R., Thorpe, A. K., Chandanpurkar, H. A., Hanke, P. J., Hasson, N., James, S. R., Minsley, B. J., Pastick, N. J., Olefeldt, D., Walter Anthony, K. M., and Miller, C. E.: Characterizing Methane Emission Hotspots From Thawing Permafrost, Global Biogeochemical Cycles, 35, e2020GB006922, https://doi.org/10.1029/2020GB006922, 2021.

Emond, A. M., Daanen, R. P., Graham, G. R. C., Anthony, K. W., Liljedahl, A. K., Minsley, B. J., Barnes, D. L., Romanovsky, V. E., and CGG Canada Services Ltd.: Airborne electromagnetic and magnetic survey, Goldstream Creek watershed, interior Alaska, Alaska Division of Geological & Geophysical Surveys, https://doi.org/10.14509/29681, 2018.

Estop-Aragonés, C., Olefeldt, D., Abbott, B. W., Chanton, J. P., Czimczik, C. I., Dean, J. F., Egan, J. E., Gandois, L., Garnett, M. H., Hartley, I. P., Hoyt, A., Lupascu, M., Natali, S. M., O'Donnell, J. A., Raymond, P. A., Tanentzap, A. J., Tank, S. E., Schuur, E. A. G., Turetsky, M., and Anthony, K. W.: Assessing the Potential for Mobilization of Old Soil Carbon After Permafrost Thaw: A Synthesis of[14] C Measurements From the Northern Permafrost Region, Global Biogeochemical Cycles, 34, e2020GB006672, https://doi.org/10.1029/2020GB006672, 2020.

Farquharson, L., Anthony, K. W., Bigelow, N., Edwards, M., and Grosse, G.: Facies analysis of ~~yedoma~~ Yedoma thermokarst lakes on the northern Seward Peninsula, Alaska, Sedimentary Geology, 340, 25–37, https://doi.org/10.1016/j.sedgeo.2016.01.002, 2016.

Freitas, N. L., Walter Anthony, K., Lenz, J., Porras, R. C., and Torn, M. S.: Substantial and overlooked greenhouse gas emissions from deep Arctic lake sediment, Nat. Geosci., 18, 65–71, https://doi.org/10.1038/s41561-024-01614-y, 2025.

Hasson, N., Walter Anthony, K. M., Elder, C., Baptiste, D., Miller, C. E., Kholodov, A. L., Rybakov, S., Anthony, P., and Daanen, R. P.: Methane emissions show exponential inverse relationship with electrical resistivityfrom discontinuous permafrost wetlands in Alaska, AGU fall meeting 2022, Chicago, n.d.

Heslop, J. K., Walter Anthony, K. M., Sepulveda-Jauregui, A., Martinez-Cruz, K., Bondurant, A., Grosse, G., and Jones, M. C.: Thermokarst lake methanogenesis along a complete talik profile, Biogeosciences, 12, 4317–4331, https://doi.org/10.5194/bg-12-4317-2015, 2015.

Hopkins, D. M.: Thaw Lakes and Thaw Sinks in the Imuruk Lake Area, Seward Peninsula, Alaska, The Journal of Geology, 57, 119–131, https://doi.org/10.1086/625591, 1949.

Hugelius, G., Strauss, J., Zubrzycki, S., Harden, J. W., Schuur, E. A. G., Ping, C. L., Schirrmeister, L., Grosse, G., Michaelson, G. J., Koven, C. D., O'Donnell, J. A., Elberling, B., Mishra, U., Camill, P., Yu, Z., Palmtag, J., and Kuhry, P.: Improved estimates show large circumpolar stocks of permafrost carbon while quantifying substantial uncertainty ranges and identifying remaining data gaps, https://doi.org/10.5194/bgd-11-4771-2014, 26 March 2014.

Kessler, M. A., Plug, L. J., and Walter Anthony, K. M.: Simulating the decadal- to millennial-scale dynamics of morphology and sequestered carbon mobilization of two thermokarst lakes in NW Alaska, J. Geophys. Res., 117, 2011JG001796, https://doi.org/10.1029/2011JG001796, 2012.

Knoblauch, C., Beer, C., Liebner, S., Grigoriev, M. N., and Pfeiffer, E.-M.: Methane production as key to the greenhouse gas budget of thawing permafrost, Nature Clim Change, 8, 309–312, https://doi.org/10.1038/s41558-018-0095-z, 2018.

Krause, S.J.E. and Trude, T.: Deciphering cryptic methane cycling: Coupling of methylotrophic methanogenesis and anaerobic oxidation of methane in hypersaline coastal wetland sediment, Geochimica et Cosmochimica Acta, 302, 160-174, https://doi.org/10.1016/j.gca.2021.03.021, 2021.

Liu, J., Young E.D. … and Treude T.: Clumped isotopes of methane trace bioenergetics in the environment, Science advances, 11 (26), DOI: 10.1126/sciadv.adu1401, 2025.

Lotem, N., Pellerin, A., Anthony, K. W., Gafni, A., Boyko, V., and Sivan, O.: Anaerobic oxidation of methane does not attenuate methane emissions from thermokarst lakes, Limnology & Oceanography, 68, 1316–1330, https://doi.org/10.1002/lno.12349, 2023.

Maltby, J., Sommer, S., Dale, A.W., and Treude, T.: Microbial methanogenesis in the sulfate-reducing zone of surface sediments traversing the Peruvian margin, Biogeosciences, 13, 283-299, https://doi.org/10.5194/bg-13-283-2016, 2016.

Martinez-Cruz, K., Sepulveda-Jauregui, A., Casper, P., Anthony, K. W., Smemo, K. A., and Thalasso, F.: Ubiquitous and significant anaerobic oxidation of methane in freshwater lake sediments, Water Research, 144, 332–340, https://doi.org/10.1016/j.watres.2018.07.053, 2018.

Obu, J.: How Much of the Earth's Surface is Underlain by Permafrost?, JGR Earth Surface, 126, e2021JF006123, https://doi.org/10.1029/2021JF006123, 2021.

Olefeldt, D., Goswami, S., Grosse, G., Hayes, D., Hugelius, G., Kuhry, P., McGuire, A. D., Romanovsky, V. E., Sannel, A. B. K., Schuur, E. A. G., and Turetsky, M. R.: Circumpolar distribution and carbon storage of thermokarst landscapes, Nat Commun, 7, 13043, https://doi.org/10.1038/ncomms13043, 2016.

Pellerin, A., Lotem, N., Walter Anthony, K., Eliani Russak, E., Hasson, N., Røy, H., Chanton, J. P., and Sivan, O.: Methane production controls in a young thermokarst lake formed by abrupt permafrost thaw, Global Change Biology, 28, 3206–3221, https://doi.org/10.1111/gcb.16151, 2022.

Péwé, T. L.: Quaternary Stratigraphic Nomenclature in Unglaciated Central Alaska, 1975.

Post, E., Alley, R. B., Christensen, T. R., Macias-Fauria, M., Forbes, B. C., Gooseff, M. N., Iler, A., Kerby, J. T., Laidre, K. L., Mann, M. E., Olofsson, J., Stroeve, J. C., Ulmer, F., Virginia, R. A., and Wang, M.: The polar regions in a 2°C warmer world, Sci. Adv., 5, eaaw9883, https://doi.org/10.1126/sciadv.aaw9883, 2019.

Schädel, C., Schuur, E. A. G., Bracho, R., Elberling, B., Knoblauch, C., Lee, H., Luo, Y., Shaver, G. R., and Turetsky, M. R.: Circumpolar assessment of permafrost C quality

and its vulnerability over time using long-term incubation data, Global Change Biology, 20, 641–652, https://doi.org/10.1111/gcb.12417, 2014.

Schuur, E. A. G., McGuire, A. D., Schädel, C., Grosse, G., Harden, J. W., Hayes, D. J., Hugelius, G., Koven, C. D., Kuhry, P., Lawrence, D. M., Natali, S. M., Olefeldt, D., Romanovsky, V. E., Schaefer, K., Turetsky, M. R., Treat, C. C., and Vonk, J. E.: Climate change and the permafrost carbon feedback, Nature, 520, 171–179, https://doi.org/10.1038/nature14338, 2015.

Sepulveda-Jauregui, A., Walter Anthony, K. M., Martinez-Cruz, K., Greene, S., and Thalasso, F.: Methane and carbon dioxide emissions from 40 lakes along a north–south latitudinal transect in Alaska, Biogeosciences, 12, 3197–3223, https://doi.org/10.5194/bg-12-3197-2015, 2015.

Shaver, G. R., Giblin, A. E., Nadelhoffer, K. J., Thieler, K. K., Downs, M. R., Laundre, J. A., and Rastetter, E. B.: Carbon turnover in Alaskan tundra soils: effects of organic matter quality, temperature, moisture and fertilizer, Journal of Ecology, 94, 740–753, https://doi.org/10.1111/j.1365-2745.2006.01139.x, 2006.

Strauss, J., Schirrmeister, L., Grosse, G., Wetterich, S., Ulrich, M., Herzschuh, U., and Hubberten, H.: The deep permafrost carbon pool of the Yedoma region in Siberia and Alaska, Geophysical Research Letters, 40, 6165–6170, https://doi.org/10.1002/2013GL058088, 2013.

Turetsky, M. R., Abbott, B. W., Jones, M. C., Anthony, K. W., Olefeldt, D., Schuur, E. A. G., Grosse, G., Kuhry, P., Hugelius, G., Koven, C., Lawrence, D. M., Gibson, C., Sannel, A. B. K., and McGuire, A. D.: Carbon release through abrupt permafrost thaw, Nat. Geosci., 13, 138–143, https://doi.org/10.1038/s41561-019-0526-0, 2020.

Wagner, D., Gattinger, A., Embacher, A., Pfeiffer, E., Schloter, M., and Lipski, A.: Methanogenic activity and biomass in Holocene permafrost deposits of the Lena Delta, Siberian Arctic and its implication for the global methane budget, Global Change Biology, 13, 1089–1099, https://doi.org/10.1111/j.1365-2486.2007.01331.x, 2007.

Sivan, O., Adler, M., Pearson, A., Gelman, F., , Bar-Or, I., John, S. G. and Eckert W.: Geochemical evidence for iron-mediated anaerobic oxidation of methane, Limnology and Oceanography., 56, 4, 1536-1544, https://doi.org/10.4319/lo.2011.56.4.1536, 2011.

Walter Anthony, K. M., Zimov, S. A., Grosse, G., Jones, M. C., Anthony, P. M., Iii, F. S. C., Finlay, J. C., Mack, M. C., Davydov, S., Frenzel, P., and Frolking, S.: A shift of thermokarst lakes from carbon sources to sinks during the Holocene epoch, Nature, 511, 452–456, https://doi.org/10.1038/nature13560, 2014.

Walter Anthony, K. M., Lindgren, P., Hanke, P., Engram, M., Anthony, P., Daanen, R. P., Bondurant, A., Liljedahl, A. K., Lenz, J., Grosse, G., Jones, B. M., Brosius, L., James, S. R., Minsley, B. J., Pastick, N. J., Munk, J., Chanton, J. P., Miller, C. E., and Meyer, F. J.: Decadal-scale hotspot methane ebullition within lakes following abrupt permafrost thaw, Environ. Res. Lett., 16, 035010, https://doi.org/10.1088/1748-9326/abc848, 2021.

Whiticar, M.J., Faber, E. and Schoell, M.: Biogenic Methane Formation in Marine and Freshwater Environments: CO2 Reduction vs. Acetate Fermentation—Isotope Evidence. Geochimica et Cosmochimica Acta, 50, 693-709. http://dx.doi.org/10.1016/0016-7037(86)90346-7, 1986.

Whiticar, M.J.: Carbon and Hydrogen Isotope Systematics of Bacterial Formation and Oxidation of Methane. Chemical Geology, 161, 291-314. http://dx.doi.org/10.1016/S0009-2541(99)00092-3, 1999.

Zhang, T., Barry, R. G., Knowles, K., Heginbottom, J. A., and Brown, J.: Statistics and characteristics of permafrost and ground-ice distribution in the Northern Hemisphere, Polar Geography, 31, 47–68, https://doi.org/10.1080/10889370802175895, 2008.

Zimov, S. A., Voropaev, Y. V., Semiletov, I. P., Davidov, S. P., Prosiannikov, S. F., Chapin, F. S., Chapin, M. C., Trumbore, S., and Tyler, S.: North Siberian Lakes: A Methane Source Fueled by Pleistocene Carbon, Science, 277, 800–802, https://doi.org/10.1126/science.277.5327.800, 1997.

827
828
829
830
831
832
833
834
835
836
837
838
839
840
841
842
843
844
845
846
847
848
849
850
851

33